Electronic Supplementary Material (ESI) for Journal of Materials Chemistry A.

Electronic Supporting Information

Identification of catalytic activity descriptors for selective 5-Hydroxymethyl furfural electrooxidation to 2,5-Furandicarboxylic acid

William Hadinata Lie [a], Yuwei Yang [a], Jodie A. Yuwono [a,b], Constantine Tsounis [a], Muhammad Zubair, [a] Joshua Wright, [c] Lars Thomsen,[b] Priyank Kumar, [a] and Nicholas M. Bedford [a*]

a. School of Chemical Engineering, University of New South Wales, Sydney NSW 2052, Australia
b. College of Engineering and Computer Science, Australia National University, Canberra ACT, 2601, Australia
c. Department of Physics, Illinois Institute of Technology, Chicago, Illinois, 606616, USA
d. Australian Synchrotron, Australian Nuclear Science and Technology Organization

Email: n.bedford@unsw.edu.au

Experimental

Chemicals and materials

All commercially available reagents and materials were used without further purification unless otherwise stated. Nickel foam (99.9% purity) used as an electrode substrate was purchased from MTI corporation. Carbon fibre paper (AvCarb® MGL 370) was purchased from Fuel Cell Store, Texas, USA. $Co(NO_3).6\ H_2O$, $Ni(NO_3).\ 6\ H_2O$, $Cu(NO_3).6\ H_2O$, $CuSO_4$, $FeCl_2.4H_2O$, $K_3Fe(CN)_6$, $NaNO_3$, Na_2CO_3, NaOH, KOH, Triethanolamine, Hydroxymethyl furfural (HMF), 2,5-Furandicarboxylic acid (FDCA), Tetrafluoro acetic acid (TFA) were purchased from Merck-Australia | Sigma-Aldrich®. HPLC grade methanol was purchased from Honeywell Research Chemicals (Chem-Supply, NSW, Sydney, Australia). Milli Q water (18.2 MW.cm resistivities) was used for solution preparation, washing, and electrochemical measurements.

Pre-treatment of Ni-foam and carbon fibre paper

Ni-foam and carbon fibre paper (CP) substrates were cut into the desired sizes prior to sequential ultrasonication in acetone, ethanol, and isopropyl alcohol (3 minutes each) to remove any organic surface impurities. The substrates were then washed with deionised water and dried overnight in a fume hood before use.

Electrodeposition of Prussian Blue Analogue films on Ni-foam

Prussian Blue Analogue thin films were electrochemically grown on pre-treated Ni-foam substrates using a modified version of a one-step electrodeposition protocol by Hashimoto's group. [1] Three metal hexacyanoferrate derivatives were prepared using cobalt nitrate hexahydrate, nickel nitrate hexahydrate and copper nitrate hexahydrate as the main precursors. Potassium hexacyanoferrate (III) was used as the second precursor for all the films. The ratio between the main precursor and the hexacyanoferrate group was kept at a 1:1 ratio at 0.5 mM concentration each.

Using cobalt hexacyanoferrate as an example of a typical preparation; A 60 mL deposition electrolyte consisting of 0.5mM $Co\ (NO_3)_2.\ 6\ H_2O$, 0.5 mM $K_3[Fe\ (CN)_6]$, and 1.0

M $NaNO_3$ was prepared. A 3cm-by-3cm Ni-foam anode compressed to 0.06 cm at 10 MPa was cleaned ultrasonically in acetone, ethanol, and DI water before electrodeposition. This anode was used as a working electrode in a 3-electrode beaker cell. Saturated calomel (SCE) electrode was used as the reference electrode and platinum foil as the counter electrode. The deposition time was modified accordingly for each PBA variant (CoFe: 5 min, NiFe: 13 min, CuFe: 20 min) to achieve a relatively similar mass loading.

Following electrodeposition, the anodes were washed with deionised water and ethanol to remove excess traces of the electrolyte. These were then allowed to dry at room temperature overnight in a fume hood. Before electrochemical tests, the PBA/Ni-foam anodes were cycled between -0.2 V to 0.9 V vs Hg/HgO in a 60ml 1.0 M KOH solution for 40 cycles at 50 $mV.s^{-1}$ scan rate.

Hydrothermal synthesis of Co_3O_4 standard on carbon fibre paper

Co_3O_4 films were hydrothermally grown on carbon fibre paper using the synthesis protocol reported by Y. Lu et al. [2] In a typical synthesis procedure, a 60 mL solution containing 0.02 mol $Co(NO_3).6\ H_2O$ and 0.04 mol Na_2CO_3 was initially prepared. This solution is then transferred to a 100 mL Teflon lined stainless steel autoclave reactor with a 1 Following which it was heated to 100 ° C and maintained for 24 hours before cooled gradually to room temperature. The resulting Co_3O_4/ CP electrode were washed with pure ethanol and deionised water before being dried under a gentle N_2 stream overnight.

Hydrothermal synthesis of NiFe LDH standard on carbon fibre paper

NiFe Layered double hydroxides (LDHs) were hydrothermally grown on carbon fibre paper using the synthesis protocol reported by Song-Jin's group. [3] In a typical synthesis procedure, 14.9mg of $FeCl_2.4H_2O$ is mixed with 22.4 mg of Triethanolamine in a 15 mL centrifuge tube. To this mixture, 65.4 mg of $Ni(NO_3)_2.6H_2O$, 90.1 mg, and 15 mL of water are added and thoroughly mixed. This resulting solution is then poured to a 23 mL Teflon lined stainless steel autoclave reactor containing a 1×3 cm pre-treated carbon fibre paper.

The autoclave reactor is then heated to 120° C for 6 hours, before cooling slowly to room temperature. The fabricated NiFe LDH /CP electrode is then washed with pure ethanol and deionised water before being dried under a gentle N_2 stream overnight

Preparation of CuO standard and drop casting on carbon fibre paper

CuO nanoparticles were hydrothermally grown on carbon fibre paper using the synthesis protocol reported by K. Arun et al. [4] In a typical synthesis procedure, a 100 mL solution of 0.1 M $CuSO_4$ was prepared using deionised water. Subsequently, a 0.3 M NaOH solution was introduced to the 0.1 M $CuSO_4$ drop-wise using a pipette with magnetic stirring until the pH reaches 9.0. This solution is then transferred to Teflon lined stainless steel autoclave containing a 1×3 cm pre-treated carbon fibre paper. The autoclave reactor is then heated to 200 ° C for 6 hours, before cooling slowly to room temperature. Finally, the electrode is placed in a muffle furnace and annealed at 250 ° C to obtain a CuO/CP electrode

Physicochemical characterisation

Scanning electron micrographs (SEM) of the deposited catalyst films were obtained using an FEI Nova SEM230 microscope with an accelerating voltage of 5kV. Transmission electron microscopy (TEM) images, scanning transmission electron microscopy (STEM) images and energy-dispersive X-ray spectroscopy (EDS) maps were obtained using a JEOL JEM-F200 microscope with an accelerating voltage of 200kV. Samples for TEM imaging were prepared by drop-casting a methanol dispersion containing scrapped thin films or powders onto a carbon-coated gold grid using a micropipette and dried under atmospheric conditions. The surface chemistry of the electrodes was analysed using a Thermo Scientific ESCALAB250Xi X-Ray Photoelectron spectrometer (XPS). Additional surface composition analysis was performed using a Perkin Elmer series 400 ATR- FTIR spectrometer scanning between 600 to 4000cm^{-1} IR wavelength. Raman analysis was

performed using a Renshaw InVia2 microscope with a 532nm laser source scanning between 100 to 4000 cm^{-1}.

X-Ray Absorption Spectroscopy measurements

Near-edge X-Ray absorption fine structure (NEXAFS) measurements were conducted at the SXR beamline of the Australian synchrotron to probe the Co, Ni, Cu L_{III} and L_{II}-edges, as well as the O K-edge. PBA electrocatalyst films were pulse electrodeposited on carbon fibre paper for partial electron yield (PEY) detection. All NEXAFS data reduction and processing was performed using the QANT program. [5, 6] XAS measurements at the Co, Ni and Cu K-edges were conducted in fluorescence mode at the 10-ID-B beamline of the Advanced Photon Source (APS), Argonne (USA). Data were recorded from 100 eV below to 800 eV above the edge of the Co K-edge (7708.9 eV) , Ni K-edge (8333 eV) and Cu K-edge (8979 eV) respectively. For each sample, a set of 16 repeat scans were recorded. The XAS raw scans were averaged and processed using the Athena software to subtract the pre-edge line and post-edge baseline contributions. [7] The extracted EXAFS oscillations were k_3-weighted, and Fourier transformed to the r-space for k = 2.3–13.3 Å. The fittings of the k_3-weighted EXAFS data in the r-space (1.5–3.0 Å) were performed using the Artemis program. Established bulk crystal structures for CoOOH , $Ni(OH)_2$, ,CuO, and $Cu(OH)_2$ were used to generate the M-O and M-M contributions for the relevant samples. An amplitude reduction factor S_0^2 of 0.76 0.84, 0.90 were used for Co ,Ni , Cu K-edges respectively as determined by corresponding metal foils fits.

Computational details

All calculations were conducted by periodic density functional theory (DFT) analyses with the Vienna ab initio simulation package (VASP) code.[8, 9] The electron-ion interactions were calculated with the projected augmented wave (PAW) method. [10, 11] The exchange-correlation energies were described using the generalised gradient approximation (GGA) with the Perdew-Burke-Ernzerhof (PBE) functional. [12] The wavefunction were expanded with a kinetic energy cut-off of 500 eV. Reciprocal lattice integrations in the Brillouin zone

using the Monkhorst-Pack scheme of 7×7×1 were used. Geometrical optimizations were calculated by relaxing all ionic position and supercell vectors until the Hellman-Feynmann forces were less than 0.03 eV Å. Dispersion energy corrections were performed using the Grimme method. [13]

The CoOOH, NiOOH, and $Cu(OH)_2$ surfaces were built using 4×4 supercells. The vacuum thickness of 20 Å was added to remove periodic interactions between slabs in the z-axis. Free energy calculations for the reduction reactions of HMF to HMFCA and FFCA to FDCA along with hydrogenation of oxyhydroxide surfaces were computed using the standard hydrogen electrode (SHE) method. In this study, the computation of reaction mechanisms and their free energy profiles was performed implicitly, using the following physical mechanisms:

CoOOH + HMF ⟶ CoOOH + HMFCA ⟶ CoOOH + FFCA ⟶ CoOOH + FDCA

NiOOH + HMF ⟶ NiOOH + HMFCA ⟶ NiOOH + FFCA ⟶ NiOOH + FDCA

CuO + HMF ⟶ CuO + HMFCA ⟶ CuO + FFCA ⟶ CuO + FDCA

The role of Fe was investigated by introducing it as a substitutional dopant in the CoOOH, NiOOH, and $Cu(OH)_2$ structures. The density of states calculations for undoped and doped systems were then performed to understand the correlation between d-band center and catalysts activity/selectivity.

Electrochemical measurements

Electrochemical measurements were done using a divided glass H-cell connected to a CHI760E workstation (CH Instruments Inc.) in 1M KOH at 25 °C (pH 14.0) separated by an anion exchange membrane (Fumatech). A Hg/HgO (0.1 M KOH) reference electrode and a platinum foil (1×1cm) counter electrode were used. The fabricated electrode was used as the working electrode with a depth of 2.5 cm submerged in the electrolyte solution.

Electrocatalytic activity of the electrodes for HMF oxidation was studied using Linear sweep voltammetry (LSV) in the 1.0 M KOH solution with and without HMF (10mM). An open circuit potential at the rate of 50mV/s was applied in the positive direction for the LSV studies. The potential recorded was converted to V (vs. RHE) using Eqn. (1).

$$E(\text{vs. RHE})\text{mV} = E(\text{vs. Hg/HgO}) + 0.059(\text{pH}) + 0.098\text{V} \qquad (1)$$

$$\text{ECSA} = \frac{C_{dl}}{C_s} \qquad (2)$$

The electrochemically active surface area (ECSA) of the anodes were determined using Eqn. (2). Where the double layer capacitance (C_{dl}) is the slope of the current-scan rate curve obtained from CV measurements in the non-faradaic double layer region. The specific capacitance (C_s) used was 0.040 mF.cm^{-2} based on previous measurements done on metal oxide electrocatalysts in 1.0 M KOH solution. [14] The current density for each electrode in the polarisation curves for OER and HMF oxidation was normalised against the calculated ECSA values.

Constant potential electrolysis was conducted at 1.42 V vs RHE at a HMF concentration of 10 mM. Aliquots of the anode electrolyte were taken from the cell directly after the addition of HMF at 10-minute intervals for HPLC analysis.

Product analysis of 5-HMF electrooxidation

Chromatographic analysis of HMF and FDCA was conducted using a Shimadzu© LC-20-AD HPLC system interfaced with a photodiode array detector. The analytes were separated on a Kinetex EVO column (5µm 150mm x 4.6mm, Phenomenex, Sydney, NSW, Australia). The HPLC technique is a 10-minutes isocratic run using a mobile phase composed of 0.1% (v/v) TFA in 5% (v/v) methanol in Milli Q water. The column oven was set at 60 °C. The flow rate and injection volume were 1 mL/min and 10 µL, respectively. Identification of the different compounds was monitored at 265nm, and the absorption spectra at 283nm and 263nm were used for quantification of corresponding 5-HMF and FDCA.

Stock standard solutions of 5-HMF, HMFCA, FFCA, FDCA (10 mM) were prepared in 0.1% (v/v) TFA in 5% (v/v) methanol in a UV-free laboratory. Stock solutions and standard calibrants were prepared fresh on the day of analysis. A 7-point external calibration curve

had a range from 0.5 µM to 1 mM. Aliquots from the H-Cell were diluted 10-fold with the mobile phase solution before HPLC analysis. The conversion of HMF, product yield and faradaic efficiency of the electrolyser were determined using equations (3-5)

$$\text{HMF conversion } (\%) = \frac{\text{Moles of HMF consumed}}{\text{Initial moles of HMF}} \times 100\% \quad (3)$$

$$\text{Product yield (x) } (\%) = \frac{\text{Moles of x formed}}{\text{Initial moles of HMF}} \times 100\% \quad (4)$$

$$\text{Faradaic efficiency * } (\%) = \frac{\text{Moles of x formed}}{\text{Charge}/6F} \times 100\% \quad (5)$$

Where, x= HMFCA, FFCA or FDCA

F= Faraday constant (96485.3329 $C.mol^{-1}$)

Supporting characterisation data

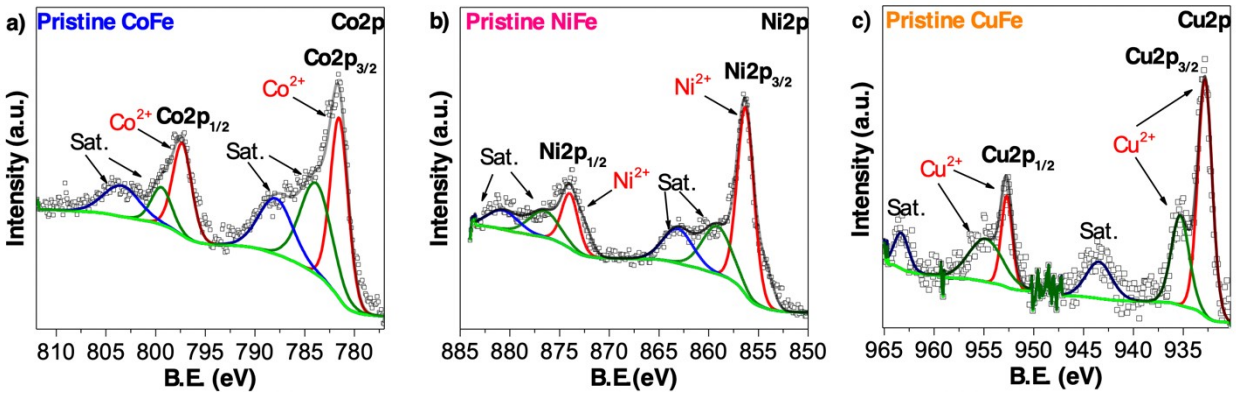

Fig S 1: Deconvoluted XPS a) Co2p, b) Ni2p , c) Cu2p spectra for pristine CoFe , NiFe, and CuFe PBA films grown on Ni-foam

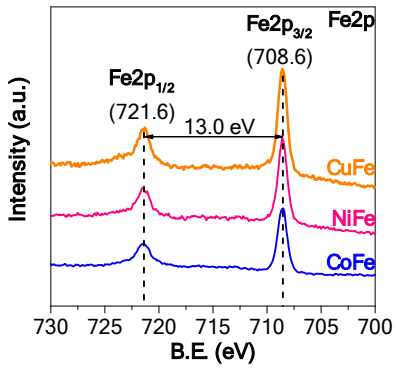

Fig S 2: High resolution XPS scans of Fe2p region for pristine CoFe, NiFe, and CuFe PBA films pulse-electrodeposited on Ni-foam substrate

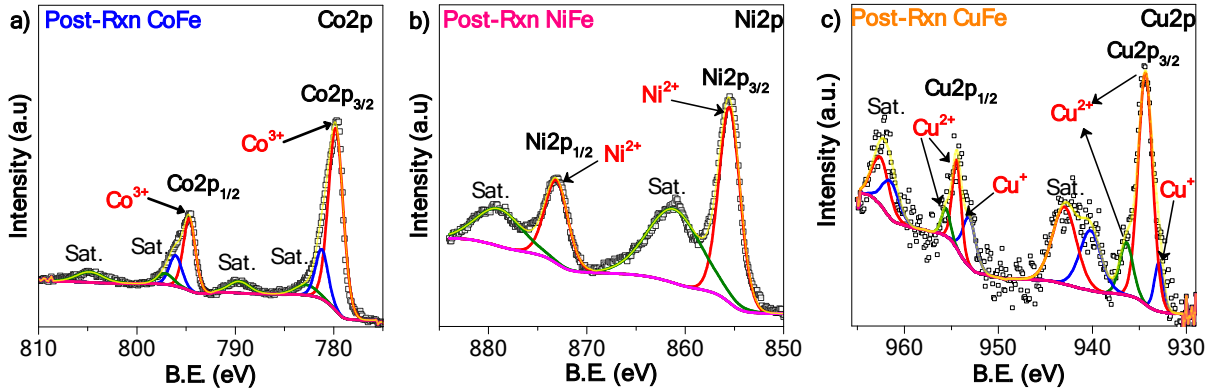

Fig S 3: High resolution XPS a)Co2p , b) Ni2p, and c) Cu2p spectra of CoFe, NiFe, and CuFe PBA films obtained after reaction in 1.0 M KOH

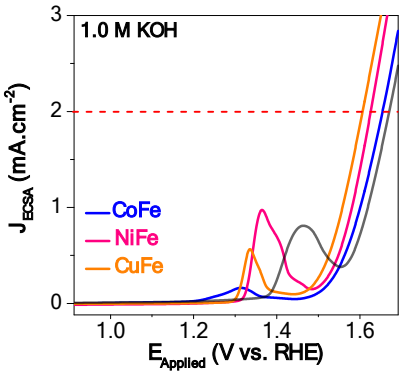

Fig S 4: LSV plots of pre-cycled CoFe, NiFe, and CuFe PBA /NF anodes with plain Ni-foam measured in 1.0 M KOH at a scan rate of 5 mV.s^{-1}

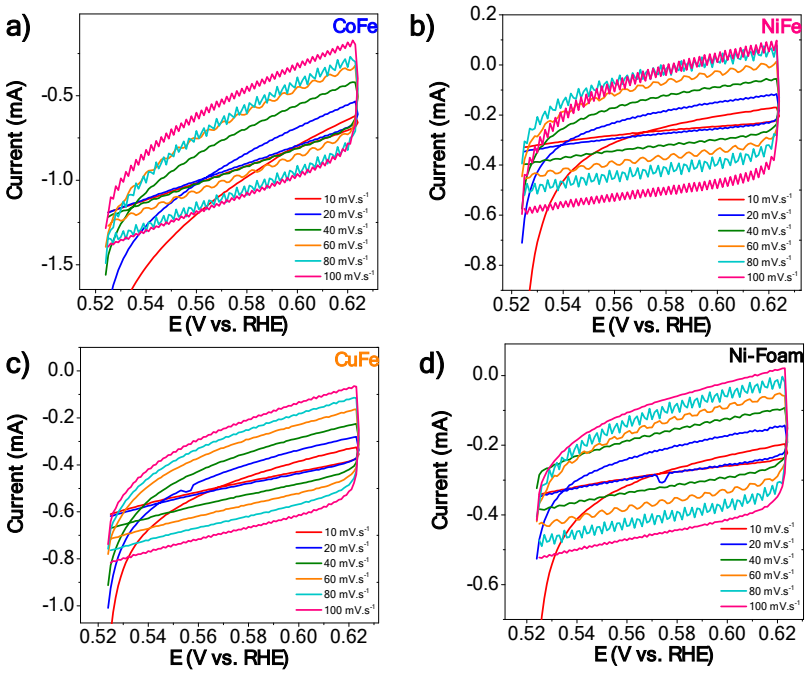

Fig S 5: CV plots of a) CoFe ,b) NiFe, c) CuFe PBA/Ni-foam electrodes and d) plain Ni-foam measured between 0. 524 V vs. RHE and 0.624 V vs. RHE in 1.0 M KOH at various scan rates from 10 mV.s^{-1} to 100 mV.s^{-1}

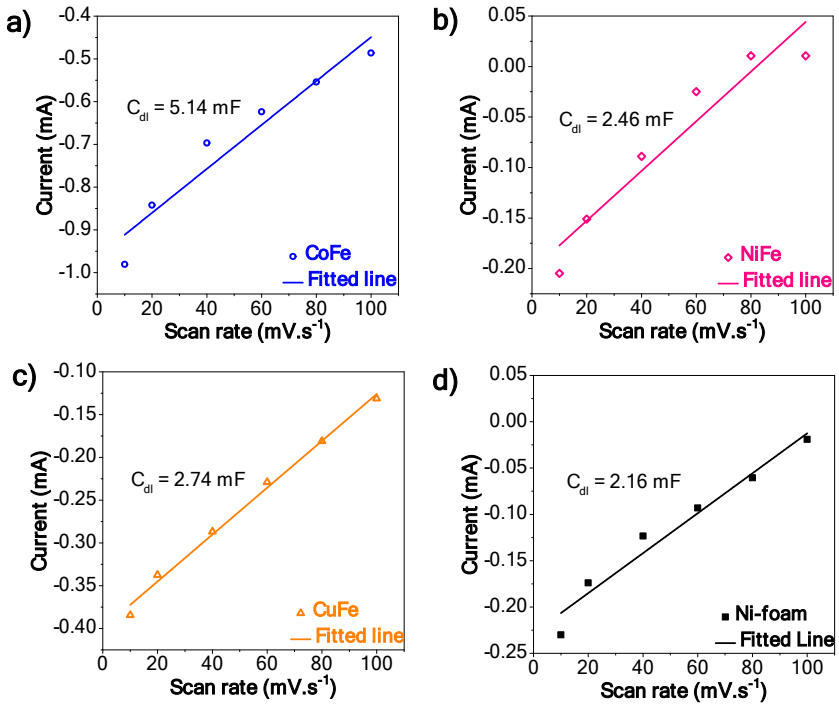

Fig S 6: Corresponding C_{dl} plots obtained from CV plots in Fig. S 5

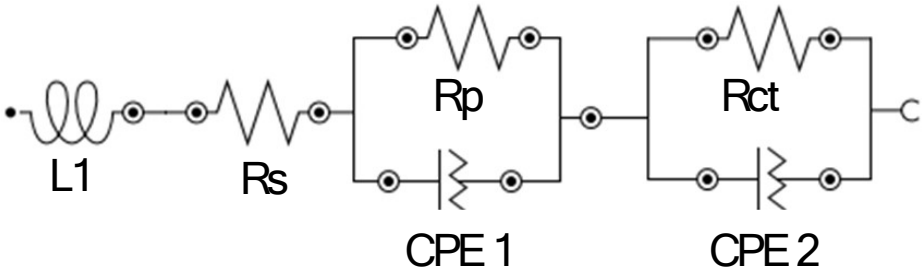

Fig S 7: Equivalent circuit model used in EIS fitting from NOVA 2.1 software

Table S 1: EIS fit parameters obtained from experimental Nyquist data

Element	Parameter	Value (CoFe)	Value (NiFe)	Value (CuFe)	Units
L1	L	5.96E-07	5.93E-07	5.66E-07	H
Rs	R	0.912	0.893	0.928	Ω
Rp	R	0.790	1.18	1.00	Ω
CPE	Y0	1.49	2.09	0.207	$mMho*s^N$
	N	1.10	1.10	0.881	
Rct	R	0.693	1.18	0.318	Ω
CPE 2	Y0	0.389	0.517	0.285	$mMho*s^N$
	N	0.767	0.655	0.615	
	χ^2	0.0778	0.0647	0.0383	

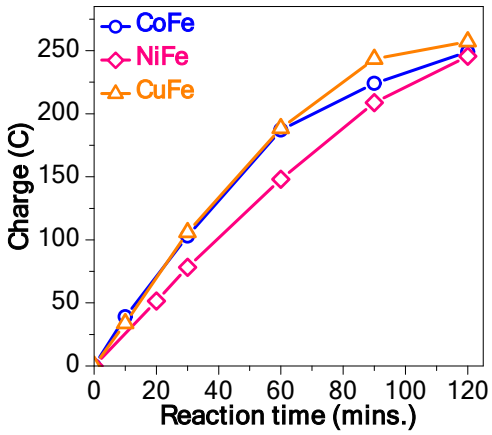

Fig S 8: Charge vs. reaction time plots of CoFe, NiFe, CuFe PBA/NF anodes during constant potential oxidation of 10 mM HMF at 1.42 V vs. RHE

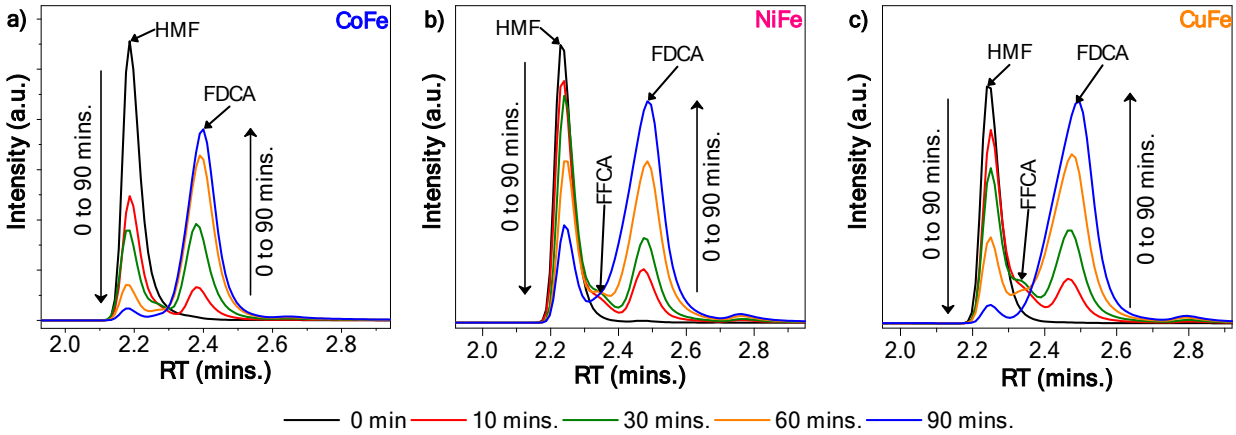

Fig S 9: HPLC chromatogram profiles of a) CoFe, b) NiFe, and c) CuFe PBA/NF anodes of aliquots recorded during constant potential oxidation of 10 mM HMF in 1.0 M KOH at 1.42 V vs. RHE during 90 minutes

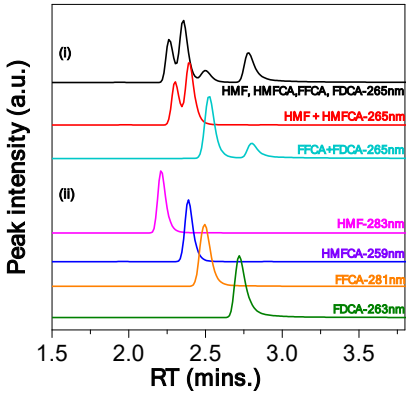

Fig S 10: HPLC Chromatograms (i) showing peaks of HMF, HMFCA, FFCA and FDCA mixed standards when monitored at 265 nm. The chromatograms (ii) showing the peak of each compound monitored at its maximum spectrum, e.g FDCA peak at 263 nm.

Table S 2: Brief comparison of reported HMF electrooxidation performance

Anode material	Electrolyte/ Conc. (M)	E_{onset} (V_{RHE})	$E_{applied}$ (V_{RHE})	Reaction time (hr.) or Charge passed (C)	FDCA Yield (%)	FE (%)	Ref.
Pt foil	0.1 mM NaOH	n/a	2.1	4 hrs.	7.69	26.5	[15]
Au_7/Pd_7	0.1 M KOH[i]	n/a	0.82	2 hrs.	11.1	83.8	[16]
Pd_7/Au_7	0.1 M KOH[i]	0.13	0.82	2 hrs.	10.1	85.8	[16]
CoFe PBA/NiF	**1.0 M KOH**	**1.23**	**1.42**	**224 C (90 min.)**	**68.5**	**90.5**	**This work**
CoOOH/FTO	0.1 M KOH[i]	~0.95	1.56	22 hrs.	35.1	35.1	[17]
CoB/NiF	1.0 M KOH	1.30	1.42	1 hr. 17 min.	~94.0	~98.0	[18]
CoP/NiF	1.0 M KOH[ii]	~0.1	1.30	60 min.	96.0	96.0	[19]
NiFe PBA/NiF	**1.0 M KOH**	**~1.30**	**1.45**	**209 C (90 min.)**	**61.4**	**80.6**	**This work**
NiOOH/FTO	0.1 M KOH[i]	1.22	1.47	4.7 hrs.	96	96	[17]
Vertical Ni NS	0.1 M KOH	~1.33	1.36	43.3 C	99.4	99.7	[20]
hP-Ni/NF	1.0 M KOH	<1.30	1.42	2.5 hrs.	95	98	[21]
Ni_3N@C	1.0 M KOH	1.32	1.45	174 C	98	99	[22]

CuFe PBA/NiF	**1.0 M KOH**	**~1.28**	**1.42**	**243 C (90 min.)**	**87.6**	**97.4**	**This work**
Nanocrystalline CuF	0.1 M KOH[i]	1.25	1.65	41 C	96.4	95.3	[23]
CuO NW/CuF	0.1 M KOH[i]	~1.30	1.64	1.5 hrs	90.9	90.4	[24]
$Cu(OH)_2$ NW/CuF	0.1 M KOH[i]	~1.40	1.69	3.4 hrs	80.3	80.5	[24]
$Cu(OH)_2$/ C	1.0 M KOH[i]	n/a	1.45	90 C	71.2	77.2	[25]

**10 mM HMF was added unless otherwise stated, i=5mM HMF, ii=20mM HMF was added*

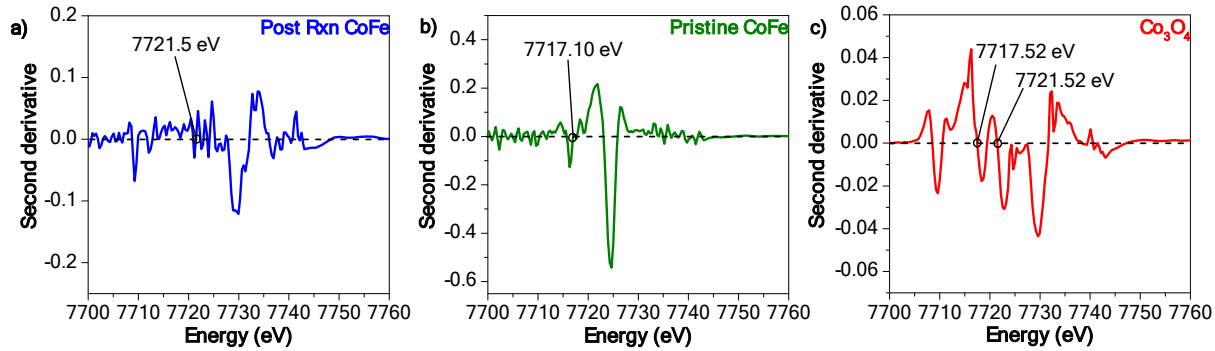

Fig S 11: Second derivative Co *K*-edge XANES spectra of a) post-reaction and b) pristine CoFe films compared against a c) prepared Co_3O_4 reference

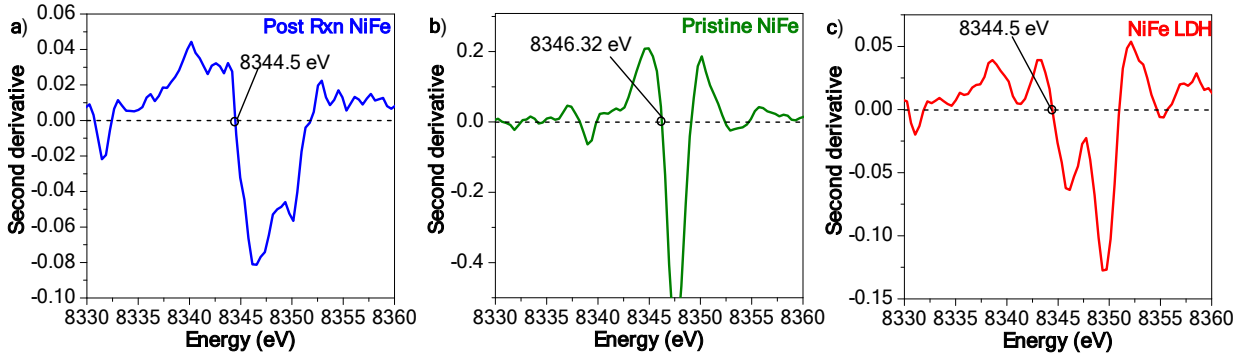

Fig S 12: Second derivative Ni *K*-edge XANES spectra of a) post-reaction and b) pristine NiFe films compared against a c) prepared NiFe LDH reference

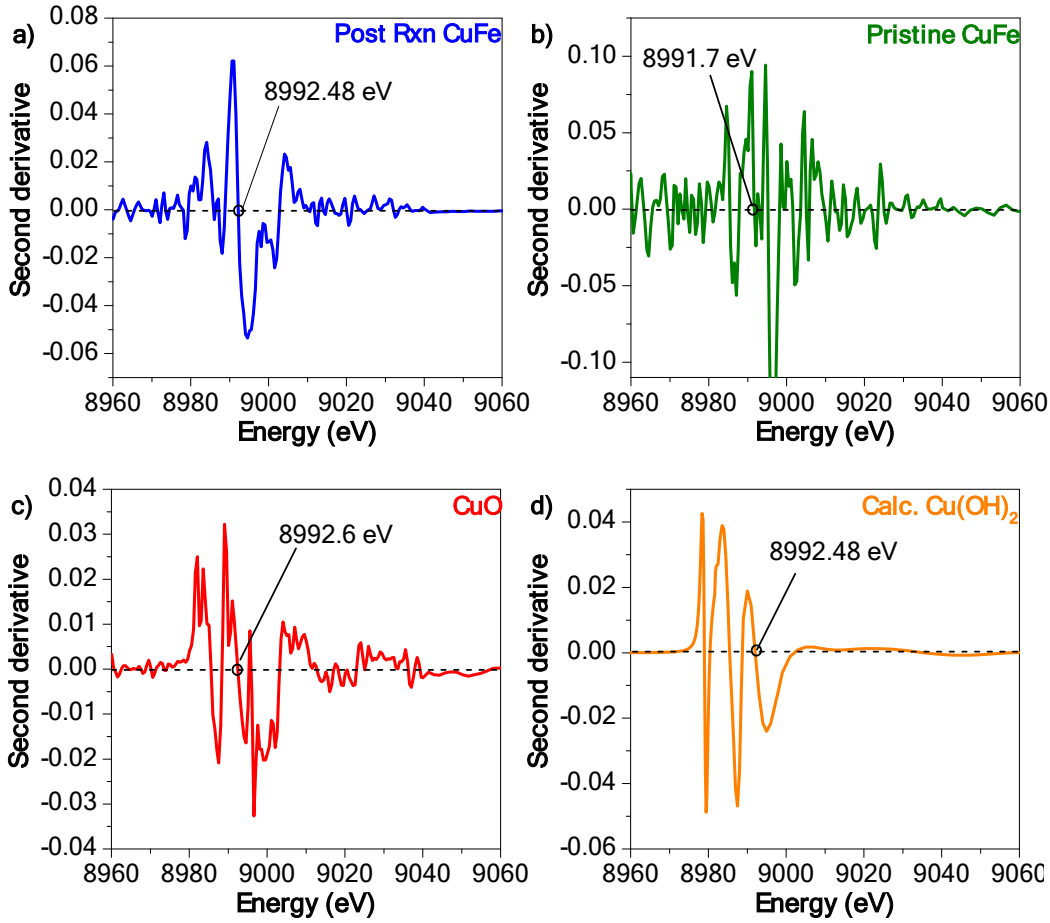

Fig S 13: Second derivative Cu *K*-edge XANES spectra of a) post-reaction and b) pristine CuFe films compared against a c) prepared CuO reference, and d) calculated $Cu(OH)_2$ spectra

The $Cu(OH)_2$ XANES and EXAFS spectra are simulated using FEFF 9.6 software with an experimentally proven $Cu(OH)_2$ structure reported by Oswald et al.[26] The cif. file used for the simulation was obtained from the URL:http://www.crystallography.net/cod/9007849.html

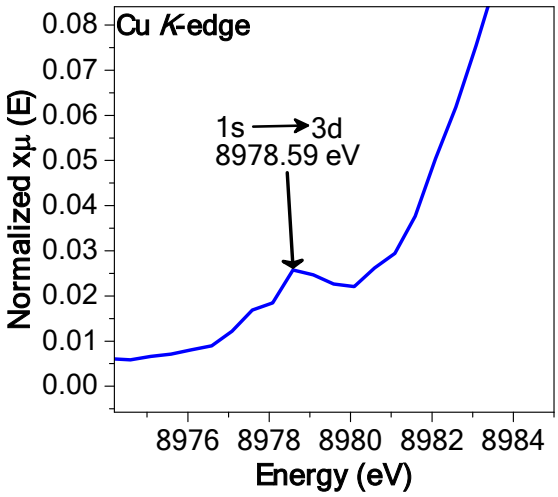

Fig S 14: Magnified XANES spectra of post-reaction CuFe film showing pre-edge peak

Table S 3: Summary of structural parameters obtained from EXAFS data

	Sample		Post-reaction CoFe
Co K-edge	Coordination number	Co-O	5.21 ± 0.431
		Co-Co	6.03 ± 0.588
	Bond length (Å)	Co-O	1.92 ± 0.00714
		Co-Co	2.86 ± 0.00659
	Debye Waller factor (Å^2)	Co-O	0.00366
		Co-Co	0.00600
	R-factor		0.0006
			Post-Reaction NiFe
Ni K-edge	Coordination number	Ni-O	6.37± 0.509
		Ni-Ni	1.08± 0.735
	Bond length (Å)	Ni-O	2.05± 0.0153
		Ni-Ni	3.10± 0.0176
	Debye Waller factor (Å^2)	Ni-O	0.00735
		Ni-Ni	0.00400
	R-factor		0.004
			Post-Reaction CuFe
Cu K-edge	Coordination number	Cu-O	3.95± 0.388
		Cu-Cu	0.870 ± 0.702
	Bond length (Å)	Cu-O	1.97 ± 0.00761
		Cu-Cu	2.92± 0.0262
	Debye Waller factor (Å^2)	Cu-O	0.00530
		Cu-Cu	0.00824
	R-factor		0.003

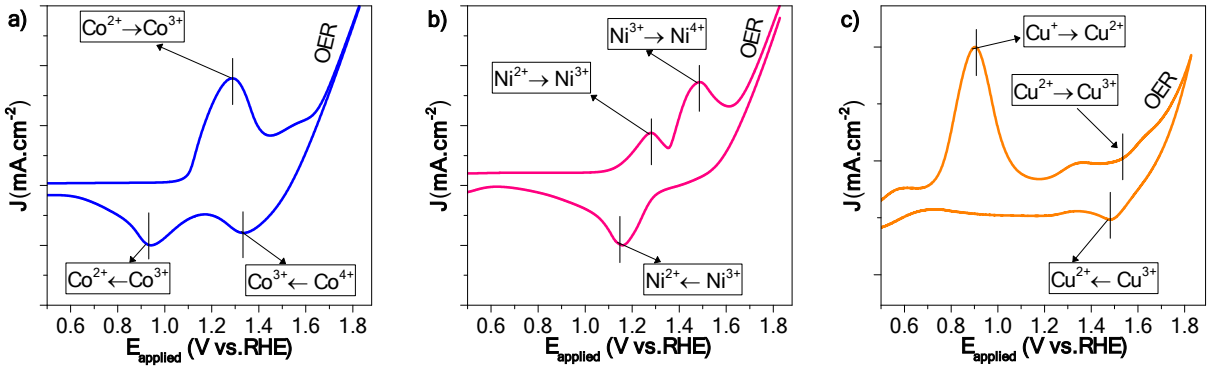

Fig S 15: CV scans of stable post-reaction a) CoFe, b) NiFe, and c) CuFe PBA films grown on carbon paper in 1.0 M KOH at 50 $mV.s^{-1}$ scan rate. Current densities are normalised against geometric surface area of carbon paper substrate

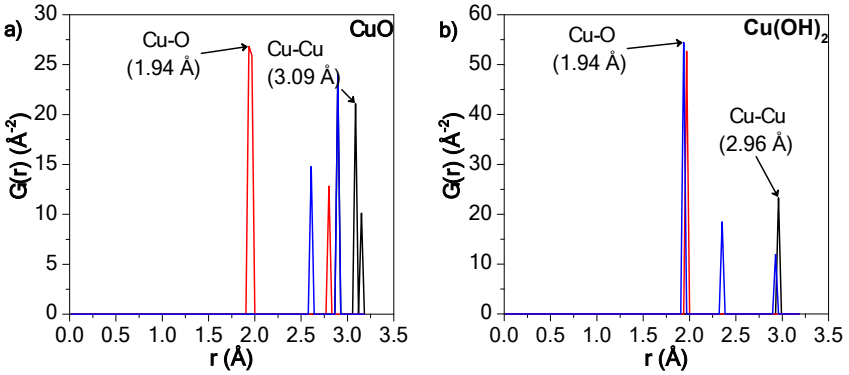

Fig S 16: Pair distribution functions of a) CuO and b) $Cu(OH)_2$ reference samples

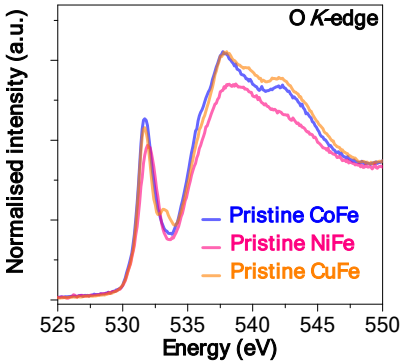

Fig S 17: Normalised O K-edge XANES plots of pristine PBA films

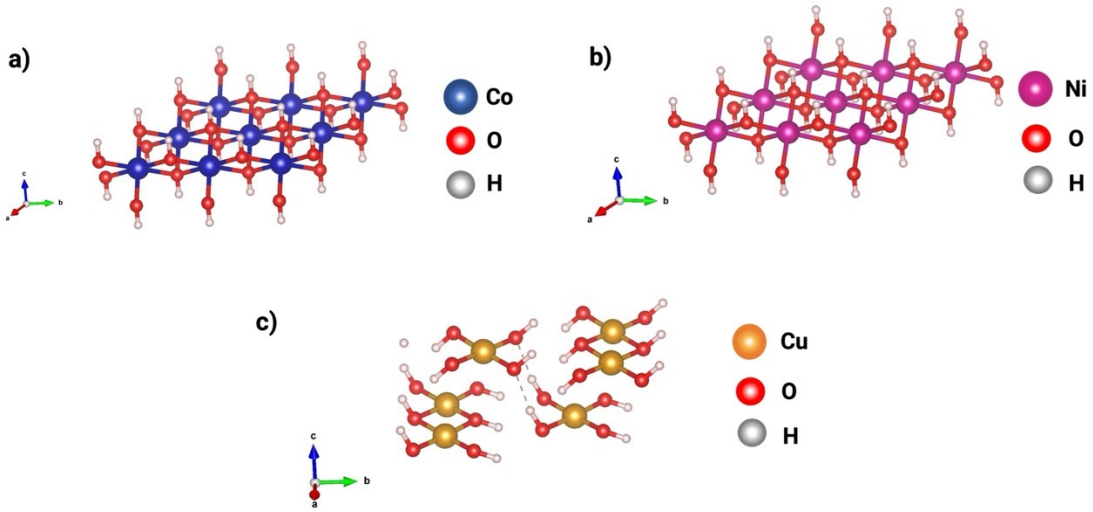

Fig S 18: a) CoOOH, b) NiOOH, and c) $Cu(OH)_2$ surface models used in DFT calculations

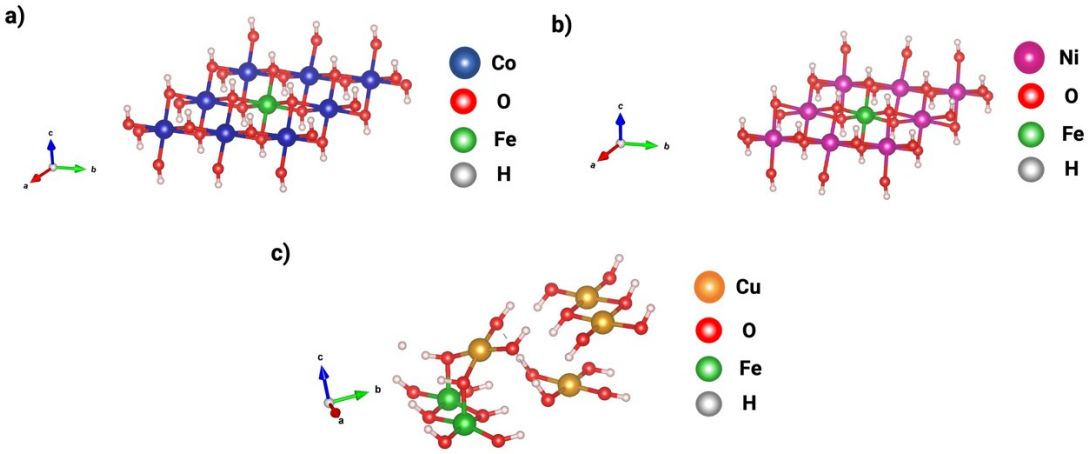

Fig S 19: Fe-doped surface models of a) CoOOH, b) NiOOH, and c) $Cu(OH)_2$ used in DFT calculations

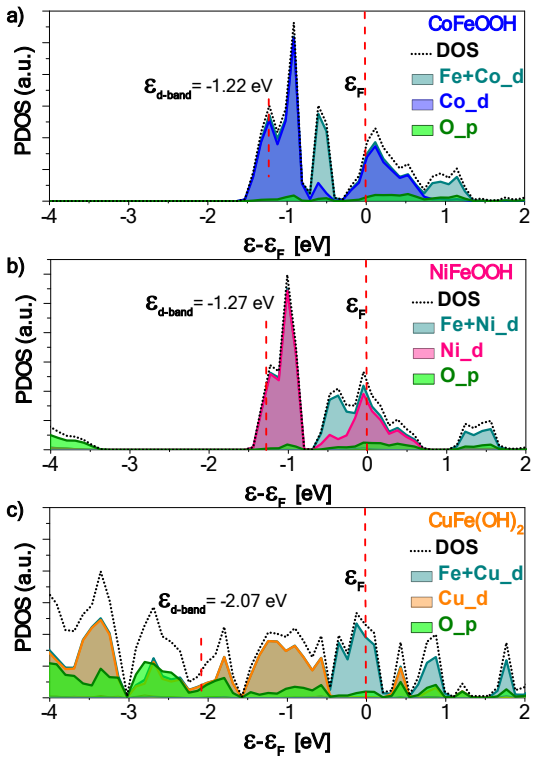

Fig S 20: Projected density of states (DOS) of PBA-derived CoOOH, NiOOH, $Cu(OH)_2$ surfaces with Fe introduced as an intersitial dopant as calculated by density functional theory (DFT). ε-ε_F is the energy position of the spectra relative from the fermi level (ε_F) indicated by the black horizontal dash line,

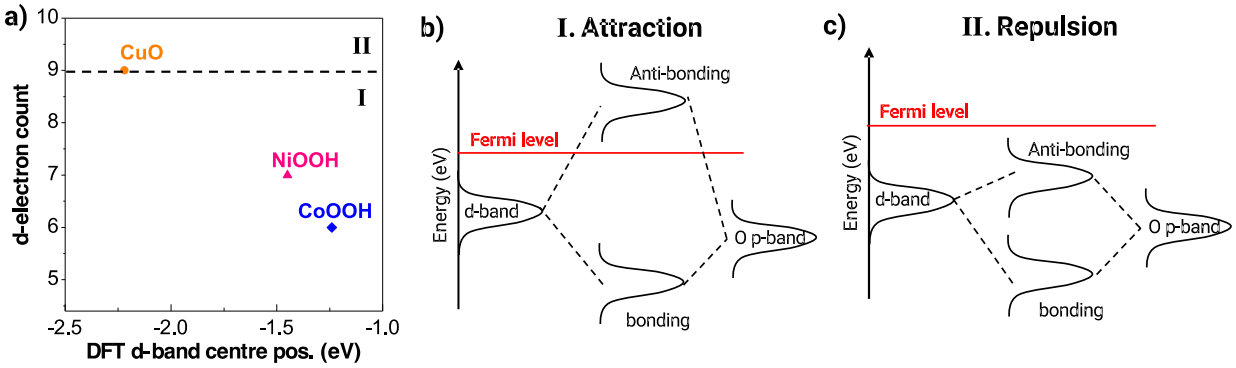

Fig S 21: a) Relationship between d-electron count and DFT-calculated d-band centre in CoOOH, NiOOH, and CuO | Schematic Illustration of the interaction between two electronic states in b) CoOOH and NiOOH, and c) CuO active phases.

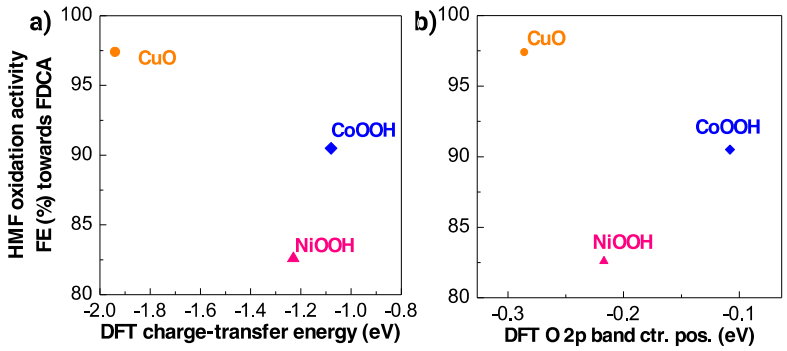

Fig S 22: Relationship between HMF oxidation activity with a) DFT- calculated charge transfer energy and b) O 2p band centre positions in CoOOH, NiOOH ,and CuO active phases

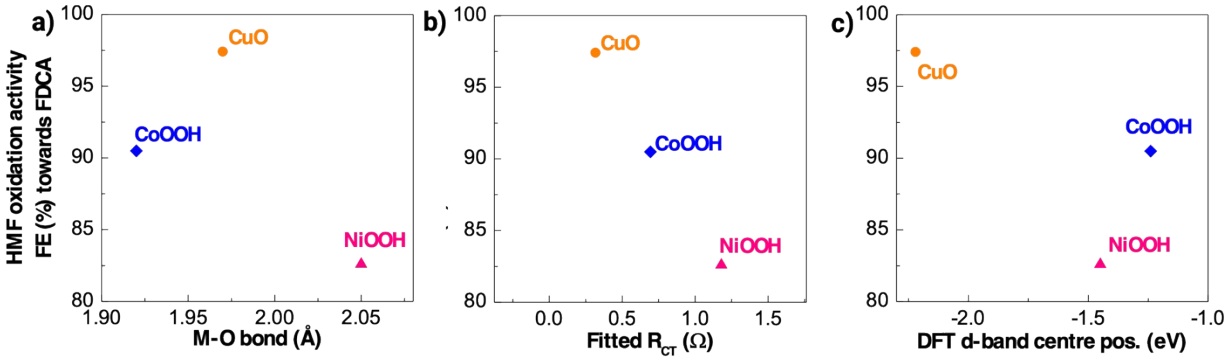

Fig S 23: Relationship between HMF oxidation activity with a) fitted EXAFS M-O bond length, b) fitted R_{CT} and c) DFT-calculated d-band centre in CoOOH, NiOOH, and CuO active phases.

Table S 4: DFT calculated O2p band centres and unoccupied metal 3d band with corresponding charge transfer energies of PBA-derived active phases during HMF oxidation

PBA precursor	Proposed active phase	O2p band centers	Unoccupied metal 3d band centers	Charge transfer energy
CoFe	CoOOH	-0.180	-1.26	-1.08
NiFe	NiOOH	-0.217	-1.44	-1.23
CuFe	CuO	-0.286	-2.22	-1.94

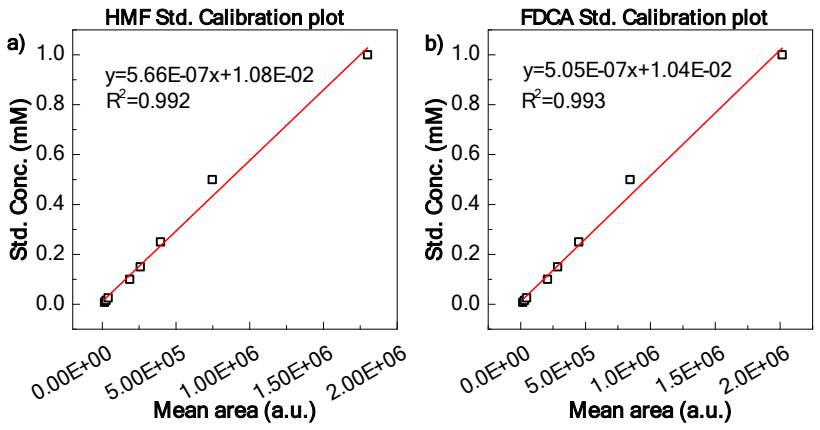

Fig S 24: a) HMF standard calibration plot and b) FDCA standard calibration plot for CoFe/NF experimental data

Table S 5: Signal intensities obtained from the HPLC were used for calculating the HMF concentration between 0 to 120 mins during constant potential electrolysis at 1.42 V_{RHE} for CoFe/NF

Time (mins)	Charge (C)	Peak Area (a.u)	Concentration (mM)	Mean (mM)	Std Dev
0	0	1856071	10.6	10.2	5.29E-01
		1723871	9.87		
		1949930	11.1		
10	39	1745038	9.98	9.82	1.27E-01
		1700363	9.73		
		1732141	9.91		
30	103	960927	5.55	5.41	1.79E-01
		901534	5.21		
		950258	5.49		
60	177	448794	2.65	2.64	1.31E-02
		444572	2.62		
		448292	2.65		
90	224	157197	1.00	1.06	7.04E-02
		181750	1.14		
		165987	1.05		
120	249	64602	0.47	0.49	2.36E-02
		66627	0.49		
		72629	0.52		

Table S 6: Signal intensities obtained from the HPLC were used for calculating the FDCA concentration between 0 to 120 mins during constant potential electrolysis at 1.42 V_{RHE} for CoFe/NF

Time (mins)	Charge (C)	Peak Area (a.u)	Concentration (mM)	Mean (mM)	Std Dev
0	0	-	-	-	-
10	39	166245	0.944	0.92	2.33E-02
		157175	0.898		
		160220	0.913		
30	103	554595	2.91	2.85	8.11E-02
		525583	2.76		
		552047	2.89		
60	177	1148358	5.90	5.93	5.80E-02
		1145228	5.89		
		1166491	6.00		
90	224	1333128	6.84	6.99	2.24E-01
		1533223	7.85		
		1395826	7.15		
120	249	1530955	7.84	8.12	5.94E-01
		1642717	8.40		
		1766174	9.02		

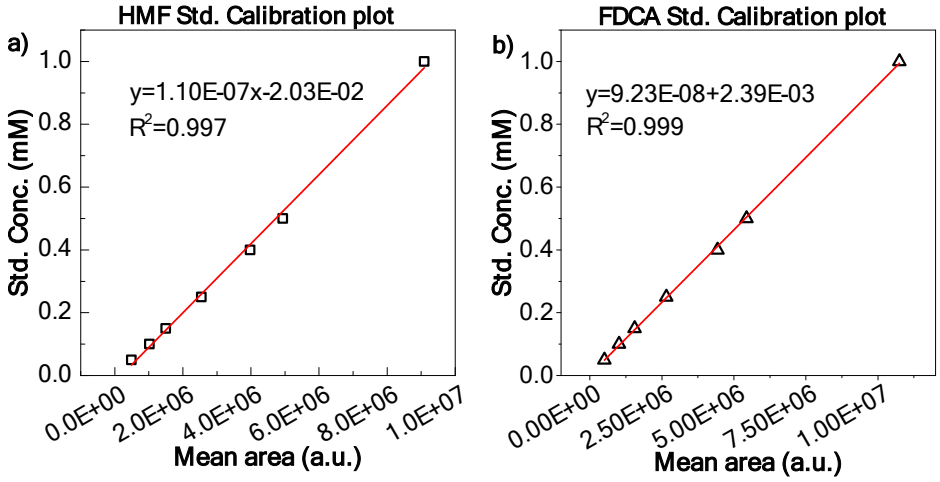

Fig S 25: a) HMF standard calibration plot and b) FDCA calibration plot for NiFe/NF and CuFe/NF experiment data during constant potential oxidation of 10 mM HMF at 1.42 V vs. RHE

Table S 7: Signal intensities obtained from the HPLC were used for calculating the HMF concentration between 0 to 120 mins during constant potential electrolysis at 1.42 V_{RHE} for NiFe/NF

Time (mins)	Charge (C)	Peak Area (a.u)	Concentration (mM)	Mean (mM)	Std Dev
0	0	8268309	8.89	9.70	2.20E-02
		8983943	9.68		
		9023687	9.72		
		8999485	9.70		
20	52.0	7746801	8.32	8.34	1.89E-02
		7776399	8.35		
		7776679	8.35		
30	79.0	7020607	7.52	7.52	4.40E-03
		7026990	7.53		
		7027985	7.53		
60	149	2981098	3.08	3.06	4.16E-02
		2921313	3.01		
		2991378	3.09		
90	209	1270865	1.19	1.19	2.31E-03
		1266833	1.19		
		1269884	1.19		
120	246	442843	0.28	0.29	1.38E-03
		445016	0.29		
		445016	0.29		

Table S 8: Signal intensities obtained from the HPLC were used for calculating the FDCA concentration between 0 to 120 mins during constant potential electrolysis at 1.42 V_{RHE} for NiFe/NF

Time (mins)	Charge (C)	Peak Area (a.u)	Concentration (mM)	Mean (mM)	Std Dev

0	0	-	-	-	-
20	52.0	1300368 1319464 529141	1.23 1.24 0.51	1.23	1.25E-02
30	79.0	2113581 2101212 1314536	1.97 1.96 1.24	1.97	8.07E-03
60	149	3750529 3756788 4514917	3.49 3.49 4.19	3.49	4.08E-03
90	209	7197640 6422254 6436349	6.67 5.95 5.96	5.96	9.20E-03
120	246	8786106 8762393 8768716	8.13 8.11 8.12	8.12	1.13E-02

Table S 9: Signal intensities obtained from the HPLC were used for calculating the HMF concentration between 0 to 90 mins during constant potential electrolysis at 1.42 V_{RHE} for CuFe/NF

Time (mins.)	Charge (C)	Peak Area (a.u.)	Concentration (mM)	Mean (mM)	Std Dev

0	0	8571358	9.43	9.35	9.52E-02
		8751330	9.25		
		8587239	9.39		
10	33.9	8062291	8.67	8.67	6.04E-03
		8071337	8.68		
		8072209	8.68		
30	105.9	5387938	5.72	5.72	3.69E-03
		5384047	5.72		
		5381266	5.72		
60	188.5	1800775	1.78	1.75	1.64E-02
		1772646	1.75		
		1774939	1.75		
		1767386	1.74		
90	243.3	310919	0.14	0.14	4.02E-03
		309522	0.14		
		304005	0.13		
120	260	11317	-0.19	-0.191	1.04E-03
		9705	-0.19		
		11353	-0.19		

Table S 10: Signal intensities obtained from the HPLC were used for calculating the FDCA concentration between 0 to 90 mins during constant potential electrolysis at 1.42 V_{RHE} for CuFe/NF

Time (mins.)	Charge (C)	Peak Area (a.u.)	Concentration (mM)	Mean (mM)	Std Dev
0		-	-	-	-

	0.00				
10	33.9	495296	0.48	0.50	2.18E-02
		528646	0.51		
		494268	0.48		
30	105.9	3128859	2.91	2.91	7.60E-04
		3130024	2.91		
		3135284	2.92		
60	188.5	6671349	6.18	6.11	7.52E-02
		6507259	6.03		
		6501871	6.03		
		6517457	6.04		
90	243.3	8869863	8.21	8.19	2.76E-02
		8827627	8.17		
		8813438	8.16		
120	260	9220334	8.53	8.53	8.70E-03
		9208285	8.52		
		9226867	8.54		

Performance stability data

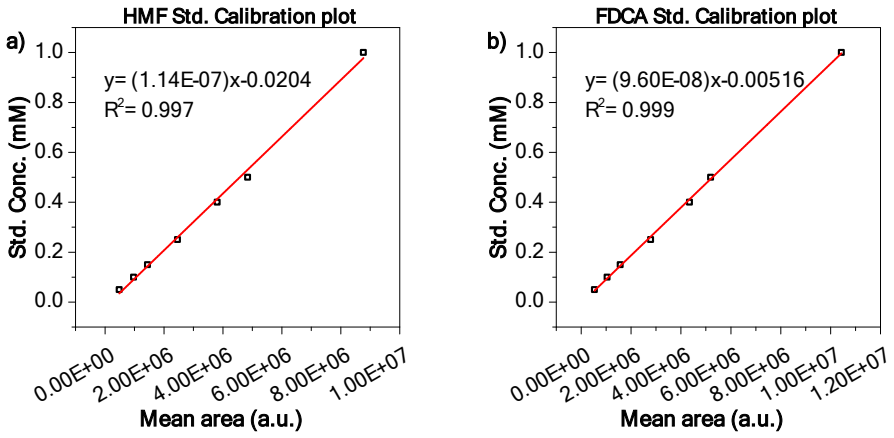

Fig S 26: a) HMF standard calibration plot and b) FDCA calibration plot for CoFe/NF and CuFe/NF experiment data during constant potential oxidation of 5 Mm HMF at 1.42 V vs. RHE

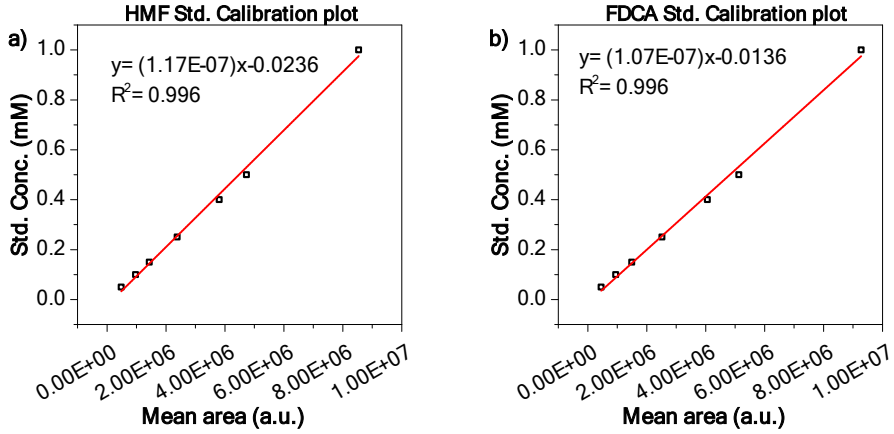

Fig S 27: a) HMF standard calibration plot and b) FDCA calibration plot for NiFe/NF experiment data during constant potential oxidation of 5 Mm HMF at 1.42 V vs. RHE

Table S 11: Signal intensities obtained from the HPLC were used for calculating the starting HMF concentration prior to 60 mins of constant potential electrolysis at 1.42 V_{RHE} for CoFe/NF

Batch cycle no.	Peak Area (a.u.)	Concentration (mM)	Mean (mM)	Std Dev
1	5146990	5.65	5.65	5.15E-03
	5138286	5.64		
	5140491	5.65		
2	4944834	5.42	5.42	1.05E-02
	4931892	5.41		
	4926871	5.40		
3	5155860	5.66	5.59	8.17E-02
	5032241	5.52		
	5030843	5.52		
4	4859912	5.33	5.32	5.96E-03
	4860398	5.33		
	4851087	5.32		

Table S 12: Signal intensities obtained from the HPLC were used for calculating the FDCA concentration after 60 mins. during constant potential electrolysis at 1.42 V_{RHE} for CoFe/NF

Batch cycle no.	Charge (C)	Peak Area (a.u.)	Concentration (mM)	Mean (mM)	Std Dev
1	113	3976626	3.77	3.76	5.93E-03
		3966088	3.76		
		3965764	3.76		
2	105	3101774	2.93	3.53	3.47E-01
		3718630	3.52		
		3736040	3.54		
3	116	3407431	3.22	3.83	3.54E-01
		4050222	3.84		
		4040031	3.83		
4	144	5006643	4.76	4.75	5.28E-03
		4996627	4.75		
		4997726	4.75		

Table S 13: Signal intensities obtained from the HPLC were used for calculating the starting HMF concentration prior to 60 mins of constant potential electrolysis at 1.42 V_{RHE} for NiFe/NF

Batch cycle no.	Peak Area (a.u.)	Concentration (mM)	Mean (mM)	Std Dev
1	4237656	4.72	4.84	2.19E-01
	4224875	4.71		
	4555587	5.09		
2	4362531	4.87	4.87	4.81E-03
	4355840	4.86		
	4363332	4.87		
3	4962232	5.57	5.56	8.60E-03
	4951192	5.56		
	4948302	5.55		
4	3552150	3.92	3.91	1.17E-02
	3532896	3.90		
	3537642	3.90		

Table S 14: Signal intensities obtained from the HPLC were used for calculating the FDCA concentration after 60 mins. during constant potential electrolysis at 1.42 V_{RHE} for NiFe/NF

Batch cycle no.	Charge (C)	Peak Area (a.u.)	Concentration (mM)	Mean (mM)	Std Dev
1	143	4501001	4.66	4.68	1.65E-02
		4531255	4.69		
		4521759	4.68		
2	147	4628238	4.80	4.81	1.71E-02
		4625153	4.79		
		4654345	4.82		
3	180	5253866	5.46	5.47	1.15E-02
		5254033	5.46		
		5272664	5.48		
4	124	3747674	3.86	3.86	1.44E-02
		3760034	3.87		
		3774582	3.89		

Table S 15: Signal intensities obtained from the HPLC were used for calculating the starting HMF concentration prior to 60 mins of constant potential electrolysis at 1.42 V_{RHE} for CuFe/NF

Batch cycle no.	Peak Area (a.u.)	Concentration (mM)	Mean (mM)	Std Dev
1	4071156	4.43	4.43	6.05E-03
	4068127	4.43		
	4060816	4.42		
2	5702946	6.29	6.28	1.21E-02
	5690567	6.27		
	5711728	6.30		
3	4644535	5.08	5.10	1.62E-02
	4672039	5.11		
	4652089	5.09		
4	5267263	5.79	6.17	4.96E-01
	5942311	6.56		
	6082508	6.72		

Table S 16: Signal intensities obtained from the HPLC were used for calculating the FDCA concentration after 60 mins. during constant potential electrolysis at 1.42 V_{RHE} for CuFe/NF

Batch cycle no.	Charge (C)	Peak Area (a.u.)	Concentration (mM)	Mean (mM)	Std Dev
1	114	4122413	3.91	3.90	8.25E-03
		4119170	3.90		
		4106181	3.89		
2	128	4658806	4.42	4.42	1.25E-02
		4664181	4.43		
		4639485	4.40		
3	127	3924377	3.72	4.32	3.47E-01
		4546335	4.31		
		4555334	4.32		
4	120	3717518	3.52	4.12	3.47E-01
		4335728	4.11		
		4349883	4.13		

Supporting references

1. O. Sato, Y. Einaga, T. Iyoda, A. Fujishima and K. Hashimoto, *J. Phys. Chem. B*, 1997, **101**, 3903-3905.
2. Y. Lu, C.-L. Dong, Y.-C. Huang, Y. Zou, Z. Liu, Y. Liu, Y. Li, N. He, J. Shi and S. Wang, *Angew. Chem. Int. Ed.*, 2020, **59**, 19215-19221.
3. W. LIU, L. Dang, Z. Xu, H.-Q. Yu, S. Jin and G. W. Huber, *ACS Catal.*, 2018.
4. K. Arun, A. Batra, A. Krishna, K. Bhat, M. Aggarwal and P. J. Francis, *Am. J. Mater. Sci*, 2015, **5**, 36-38.
5. B. Cowie, A. Tadich and L. Thomsen, 2010.
6. E. Gann, C. R. McNeill, A. Tadich, B. C. Cowie and L. Thomsen, *J. Synchrotron Radiat.*, 2016, **23**, 374-380.
7. B. Ravel and M. Newville, *J. Synchrotron Radiat.*, 2005, **12**, 537-541.
8. G. Kresse and J. Furthmüller, *Comput. Mater. Sci.*, 1996, **6**, 15-50.
9. G. Kresse and J. Furthmüller, *Phys. Rev. B.*, 1996, **54**, 11169.
10. P. E. Blöchl, *Phys. Rev. B.*, 1994, **50**, 17953.
11. G. Kresse and D. Joubert, *Phys. Rev. B.*, 1999, **59**, 1758.
12. J. P. Perdew, K. Burke and M. Ernzerhof, *Phys. Rev. Lett.*, 1996, **77**, 3865.
13. S. Grimme, J. Antony, S. Ehrlich and H. Krieg, *J. Chem. Phys.*, 2010, **132**, 154104.
14. C. C. McCrory, S. Jung, J. C. Peters and T. F. Jaramillo, *JACS*, 2013, **135**, 16977-16987.
15. K. R. Vuyyuru and P. Strasser, *Catal*, 2012, **195**, 144-154.
16. M. Park, M. Gu and B.-S. Kim, *ACS Nano*, 2020, **14**, 6812-6822.
17. B. J. Taitt, D.-H. Nam and K.-S. Choi, *ACS Catal.*, 2018, DOI: 10.1021/acscatal.8b04003, 660-670.
18. J. Weidner, S. Barwe, K. Sliozberg, S. Piontek, J. Masa, U.-P. Apfel and W. Schuhmann, *Beilstein J. Org. Chem.*, 2018, **14**, 1436-1445.
19. M. A. Suliman, K. M. Al Aqad and C. Basheer, *Molecules*, 2022, **27**, 382.
20. X. Lu, K. H. Wu, B. Zhang, J. Chen, F. Li, B. J. Su, P. Yan, J. M. Chen and W. Qi, *Angew. Chem.*, 2021, **133**, 14649-14656.
21. B. You, X. Liu, X. Liu and Y. Sun, *ACS Catal.*, 2017, **7**, 4564-4570.

22. N. Zhang, Y. Zou, L. Tao, W. Chen, L. Zhou, Z. Liu, B. Zhou, G. Huang, H. Lin and S. Wang, *Angew. Chem., Int. Ed.*, 2019, **131**, 16042-16050.
23. D.-H. Nam, B. J. Taitt and K.-S. Choi, *ACS Catal.*, 2018, **8**, 1197-1206.
24. H. M. Pham, M. J. Kang, K.-A. Kim, C. G. Im, S. Y. Hwang and H. G. Cha, *Korean J Chem Eng*, 2020, **37**, 556-562.
25. H. Chen, J. Wang, Y. Yao, Z. Zhang, Z. Yang, J. Li, K. Chen, X. Lu, P. Ouyang and J. Fu, *ChemElectroChem*, 2019, **6**, 5797-5801.
26. H.-R. Oswald, A. Reller, H. Schmalle and E. Dubler, *Acta Crystallogr. C Struct. Chem.*, 1990, **46**, 2279-2284.